Hindawi
Geofluids
Volume 2022, Article ID 6307522, 15 pages
https://doi.org/10.1155/2022/6307522

*Research Article*

# Roof-Breaking Characteristics and Ground Pressure Behavior in Deep Jurassic Coal Seams: A Thick-Plate Model and Field Measurements

**Wei Zhang,[1,2] Yandong Zhang,[2] Weisheng Zhang,[3] Liang Chen,[1,2] Fanjia Li,[4] and Kaidi Xie[2]**

[1]*State Key Laboratory of Coal Resources and Safe Mining, China University of Mining and Technology, Xuzhou 221116, China*
[2]*School of Mines, China University of Mining and Technology, Xuzhou 221116, China*
[3]*Zhengzhou Coal Mining Machinery Group Co., Ltd, Zhengzhou 450016, China*
[4]*School of Information and Control Engineering, China University of Mining and Technology, Xuzhou 221116, China*

Correspondence should be addressed to Yandong Zhang; zhangyandong@cumt.edu.cn

Received 29 July 2021; Accepted 17 September 2021; Published 23 June 2022

Academic Editor: Hualei Zhang



Roof-breaking characteristics and ground pressure behavior of the coalface are instrumental in guiding deep Jurassic coal seam mining, in particular in the Shaanxi and Inner Mongolia regions of China. A thick-plate mechanical model (TPMM) of the main roof was developed and applied to the case study of 21102 first-mined coalface (FMC) of the Hulusu Coal Mine (HCM) in the Hujirt Mining Area (HMA), China. A theoretical analysis performed via the developed model revealed that the first and periodic breaking intervals of the main roof were 40.6 and 25.0 m, respectively. The roof failure occurred in the tensile mode, was controlled by the internal stress $\sigma_x$ in the rock strata, and started from the center of the long side with the fixed support in the goaf. The field measurement of roof weighting was also performed for the coalface advance from zero to 400 m. The measurement results showed that the first weighting average interval was 41.4 m, and the average interval of periodic weighting was 22.0 m, which agreed with the theoretical calculation and proved the proposed model's feasibility. Finally, the frequency distribution features of the hydraulic support working resistance in the FMC were analyzed statistically. The results showed that the ZY10000-16/32D supports could adapt to the mining geological conditions of the FMC. However, the margin of the rated working resistance of supports was still small. Thus, roof management enhancement during the mining process was strongly recommended. These research findings could offer theoretical guidance for safe and high-efficiency production in the coal mines under similar geological conditions.

## 1. Introduction

In recent years, the development of coal resources in China has rapidly shifted to Northwestern China, especially the Inner Mongolia Autonomous Region [1]. From January to December 2020, China's northwestern coal mining areas accounted for about 70% of the total national coal output and became a forepost of China's coal industry upgrading [2–5]. A good example is the Ordos City in the Inner Mongolia Autonomous Region, in which coal production in 2018, 2019, and 2020 amounted to 616, 679, and 640 million tons, respectively.

The Dongsheng Coalfield in the Ordos City extends for about 100 km in the north-south direction and has the largest width in the east-west direction of 100 km, covering an area of about 8790 km$^2$ [6, 7]. The main coal-bearing seams in the Dongsheng Coalfield belong to the Middle Jurassic Yanan Formation, which lithology consists primarily of medium sandstone, siltstone, mudstone, and coal seam [8]. The coal seam's burial depth generally drops from north to south but increases from east to west. The coal seams mined at an early stage are generally typical shallow-buried (below 300 m) with simple geological conditions, which have been investigated theoretically

and subjected to field studies. Abundant reports have been published concerning roof-breaking characteristics, mining-induced fissure development, and ground pressure behavior [9–18]. These findings lay a theoretical foundation and offer ready technologies for the safe and high-efficiency mining of shallow-buried coal seams at an early stage. However, due to the variabilities of the burial depth of the coal seam and strata structure, the first-mined coal seams in some newly developed large-scale coal bases in the Dongsheng Coalfield have already entered the stage of deep mining [19]. One example of this is the HMA, a state planning mining area located in the midwestern part of the Dongsheng Coalfield. The main coal seams in the HMA are #2 and #3 coal seams in the upper Jurassic Yanan Formation, with a depth above 600 m. The available roof-breaking characteristics and ground pressure behavior in mining shallow-buried coal seams can no longer offer guidance for deep coal resource development in this region. It is necessary to carry out in-depth investigations into the occurrence conditions of the Jurassic deep-buried coal seam in this mining area.

The HMA is located on the border of Inner Mongolia and Shaanxi. The total planning area is about 2161 $km^2$. According to preliminary planning, this mining area is subdivided into seven mine fields, two exploration areas, and one prospective area. The total planning area is 63 Mt/a. HCM, located in the mid-southern part of the mining area, is one of the first developed in this region and has a design production capacity of 13.0 Mt/a. The burial depth of the mined coal seam is 650-900 m. The HCM is a typical newly built deep coal mine in Inner Mongolia and Shaanxi. The increased mining scope was accompanied by a series of problems: large intensity of overburdened rock activities in the stope, intense ground pressure at the coalface, and large deformation of the roadway-surrounding rocks [20]. However, there are only a few studies on roof breaking and ground pressure in this mining area [21–25].

Given this, we elaborated a TPMM for the main roof breakage in the 21102 FMC of the HCM in the HMA under the actual geological conditions. A theoretical analysis of the main roof's first and periodic breaking was performed using the established model. On this basis, we conducted a field measurement to study ground pressure behavior at the FMC. The applicability of the hydraulic supports used for this FMC was evaluated. Our research findings offer theoretical guidance for the normal mining of other coalfaces in the HCM. Moreover, these results can be utilized to guide the safe and high-efficiency coal production under similar geological conditions in the HMA.

## 2. Mining Technical Conditions for the FMC

The 21102 coalface of the HCM, the FMC in the entire mine field, is located in the first panel of the #2-1 coal seam. There are three roadways on the east wing of the mine north of the coalface. In the south, there is the fifth panel of the coal seam. The length of the coalface along the dip direction is 320 m, and that along the strike direction is 4150 m. The stoping area is 1,327,900 $m^2$. The ground surface above the coalface is hilly sand land, with an elevation of +1304 to +1328 m. The elevation of the underground coal seam roof is +673 to +694 m. The burial depth of the coalface is 626.17 to 647.91 m. The coalface under study is a typical deep-lying coalface in this region. The coal seam mined in the coalface is the #2-1 coal seam of the Jurassic Yanan Formation, with a density of about 1.31 $t/m^3$. The coal seam thickness is 1.7-3.0 m, with an average of 2.55 m, indicating a medium thickness. The coal seam is of a simple structure with slight undulation and a dip angle of 1°-3°. This coal seam is near-horizontal.

The geological structure of this coalface is also simple. The false roof of the coal seam is mainly composed of sandy mudstone, with a thickness of 0.2-0.5 m. The immediate roof comprises sandy mudstone and silty sandstone, with a thickness of 2.43-7.8 m. The main roof is composed of fine sandstone and medium sandstone, with a thickness of 13.30-23.3 m. The immediate floor comprises sandy mudstone and silty sandstone, with a thickness of 3.4-8.9 m. The stratigraphic synthesis column of the study area is shown in Figure 1. In this coalface, the full-thickness longwall mining method along the strike (with an average mining height of 2.55 m) is performed. The goaf roof is managed by using the full caving method. The hydraulic supports used in the coalface are ZY10000-16/32D two-column shield-type hydraulic supports manufactured by China Coal Beijing Coal Mining Machinery Co., Ltd. The rated working resistance of the supports is 10,000 kN, and the distance between the centers of the two supports is 1.75 m.

## 3. Mechanical Analysis of Breaking Characteristics of the Thick Sandstone Main Roof in the FMC

A goaf is formed along with the constant advance of the coalface from the open-off cut. The first breaking and weighting of the main roof occur when the roof overhang is too big. As the coalface continues to advance after the first breaking, the periodic weighting of the main roof occurs. Since the main roof of the FMC is composed of hard thick sandstone, the conventional beam model may not apply to the theoretical analysis of the roof-breaking characteristics [26]. According to the field measurement of ground pressure in the deep-buried mine near the HCM, we considered the influence of internal transverse shear stress of the plate based on the judgment criteria of the plate model. We developed the Reissner thick-plate model for the breaking of the thick sandstone main roof and performed a theoretical analysis of stress distribution in the main roof at different mining stages in the coalface. The inducing factors of the first and periodic breaking of the main roof were determined. The first and periodic weighting intervals were calculated for this coalface.

*3.1. Establishment of the TPMM for Main Roof Breaking.* Since the 21102 coalface is the FMC, the main roof can be simplified into a thick rectangular plate that has fixed support on the four sides upon the moment of the first breaking. Under this assumption, we built the TPMM for the first breaking of the main roof, as shown in Figure 2(a). After the first breaking of the main roof, broken rock masses in the goaf form a three-hinged arch. At this moment, the main roof can be reduced to a thick rectangular plate with simple support on one side and fixed support on the other three sides. Thus, the TPMM for periodic breaking of the main roof was

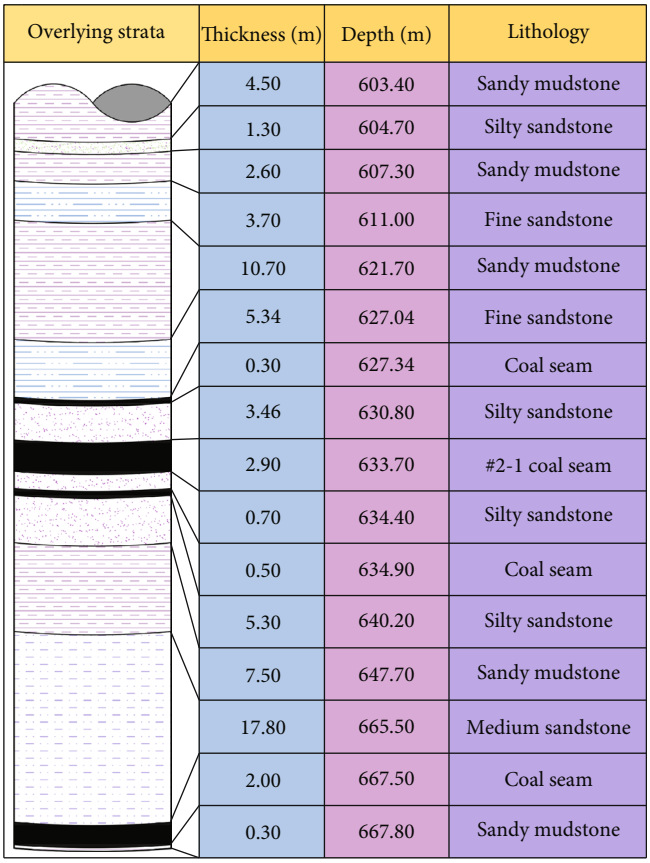

| Overlying strata | Thickness (m) | Depth (m) | Lithology |
|---|---|---|---|
| | 4.50 | 603.40 | Sandy mudstone |
| | 1.30 | 604.70 | Silty sandstone |
| | 2.60 | 607.30 | Sandy mudstone |
| | 3.70 | 611.00 | Fine sandstone |
| | 10.70 | 621.70 | Sandy mudstone |
| | 5.34 | 627.04 | Fine sandstone |
| | 0.30 | 627.34 | Coal seam |
| | 3.46 | 630.80 | Silty sandstone |
| | 2.90 | 633.70 | #2-1 coal seam |
| | 0.70 | 634.40 | Silty sandstone |
| | 0.50 | 634.90 | Coal seam |
| | 5.30 | 640.20 | Silty sandstone |
| | 7.50 | 647.70 | Sandy mudstone |
| | 17.80 | 665.50 | Medium sandstone |
| | 2.00 | 667.50 | Coal seam |
| | 0.30 | 667.80 | Sandy mudstone |

Figure 1: The stratigraphic synthesis column of study area.

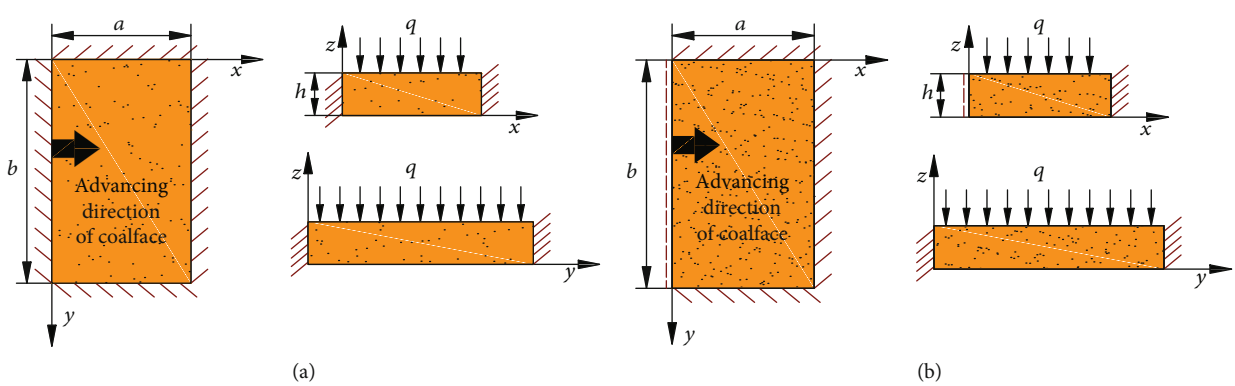


Figure 2: TPMM of the main roof breaking: (a) first breaking model and (b) periodic breaking model.

built, as shown in Figure 2(b), where $a$ and $b$ are the short and long sides of the thick rectangular plate, respectively; $h$ is its thickness; and $q$ is the load acting on the upper part of the thick rectangular plate.

According to the Reissner plate theory, the basic equations can be written as follows [27–29]:

$$D\nabla^2\nabla^2\omega = q(x,y) - \frac{(2-\mu)}{(1-\mu)}\frac{h^2}{10}\nabla^2 q(x,y), \tag{1}$$

$$\nabla^2\phi - \frac{10}{h^2}\phi = 0, \tag{2}$$

where $D$ is the bending stiffness of the main roof, $D = Eh^3/[12(1-\mu^2)]$ (N·m), $E$ is the elastic modulus of the main roof (GPa), $\omega$ is the deflection of the main roof (m), $\nabla$ is the Laplace operator, $q(x,y)$ is the loading acting on the upper part of the main roof (MPa), $\mu$ is Poisson's ratio of the main roof, $h$ is the main roof thickness (m), and $\varphi$ is the stress function within the main roof.

The expressions of the shear stress $Q$ and the bending moment $M$ for the main roof can be derived as follows:

$$Q_x = -D\frac{\partial}{\partial x}\nabla^2\omega - \frac{(2-\mu)}{(1-\mu)}\frac{h^2}{10}\frac{\partial q}{\partial x} + \frac{\partial \phi}{\partial y}, \tag{3}$$

$$Q_y = -D\frac{\partial}{\partial y}\nabla^2\omega - \frac{(2-\mu)}{(1-\mu)}\frac{h^2}{10}\frac{\partial q}{\partial y} + \frac{\partial \phi}{\partial x}, \tag{4}$$

$$M_x = -D\left(\frac{\partial^2\omega}{\partial x^2} + \mu\frac{\partial^2\omega}{\partial y^2}\right) + \frac{h^2}{5}\frac{\partial Q_x}{\partial x} - \frac{\mu}{1-\mu}\frac{qh^2}{10}, \tag{5}$$

$$M_y = -D\left(\frac{\partial^2\omega}{\partial y^2} + \mu\frac{\partial^2\omega}{\partial x^2}\right) + \frac{h^2}{5}\frac{\partial Q_y}{\partial y} - \frac{\mu}{1-\mu}\frac{qh^2}{10}. \tag{6}$$

### *3.2. Mechanical Analysis of the First Breaking Characteristics of the Main Roof*

*3.2.1. A Theoretical Analysis of the Mechanical Model Describing the First Breaking of the Main Roof.* The governing equations for the fixed support of the four sides before the first breaking of the main roof in the FMC have the following forms:

$$\begin{cases} \omega\big|_{x=0,x=a} = 0, \\ \dfrac{\partial\omega}{\partial x}\Big|_{x=0,x=a} = 0, \\ \omega\big|_{y=0,y=b} = 0, \\ \dfrac{\partial\omega}{\partial y}\Big|_{y=0,y=b} = 0. \end{cases} \tag{7}$$

Using the fixed support boundary conditions for the four sides of the main roof, the following deflection equation that satisfied the boundary conditions was derived:

$$\omega = c\left(x^2 - ax\right)^2\left(y^2 - by\right)^2. \tag{8}$$

Substituting Equation (8) and $q_0$ (the uniformly distributed load applied to the upper part of the main roof) into Equation (1), we can calculate the coefficient $c$ by the Matlab software program:

$$c = \frac{49q_0}{8D\left(7a^4 + 4a^2b^2 + 7b^4\right)}. \tag{9}$$

Substituting Equation (9) into Equation (8), we obtain the deflection function under the fixed support boundary conditions for the four sides of the main roof:

$$\omega = \frac{49q_0\left(x^2 - ax\right)^2\left(y^2 - by\right)^2}{8D\left(7a^4 + 4a^2b^2 + 7b^4\right)}. \tag{10}$$

Substituting Equation (10) into Equations (3)–(6), the shear stress function and the bending moment function of the main roof are derived as follows:

$$\begin{aligned} Q_x &= 2k\left[(6x-3a)\left(y^2-by\right)^2 + \left(x^2-ax\right)(2x-a)\left(6y^2-6by+b^2\right)\right], \\ Q_y &= 2k\left[(6y-3b)\left(x^2-ax\right)^2 + \left(y^2-by\right)(2y-b)\left(6x^2-6ax+a^2\right)\right], \\ M_x &= k\left\{\left(y^2-by\right)^2\left(6x^2-6ax+a^2+\frac{12}{5}h^2\right) + \left(6y^2-6by+b^2\right)\right. \\ &\quad \cdot \left.\left[\mu\left(x^2-ax\right)^2 + \frac{2h^2\left(6x^2-6ax+a^2\right)}{5}\right]\right\} - \frac{\mu q_0 h^2}{10(1-\mu)}, \\ M_y &= k\left\{\left(x^2-ax\right)^2\left(6y^2-6by+b^2+\frac{12}{5}h^2\right) + \left(6x^2-6ax+a^2\right)\right. \\ &\quad \cdot \left.\left[\mu\left(y^2-by\right)^2 + \frac{2h^2\left(6y^2-6by+b^2\right)}{5}\right]\right\} - \frac{\mu q_0 h^2}{10(1-\mu)}, \end{aligned} \tag{11}$$

where $k = -49q_0/4(7a^4 + 4a^2b^2 + 7b^4)$.

According to the theory of elasticity and thick-plate theory, the stress $\sigma$ in the main roof is related to the bending moment $M$ as $\sigma = 6M/h^2$. From this, we can derive the stress function of the main roof:

$$\begin{aligned} \sigma_x &= \frac{6k}{h^2}\left\{\left(y^2-by\right)^2\left(6x^2-6ax+a^2+\frac{12}{5}h^2\right) + \left(6y^2-6by+b^2\right)\right. \\ &\quad \cdot \left.\left[\mu\left(x^2-ax\right)^2 + \frac{2h^2\left(6x^2-6ax+a^2\right)}{5}\right]\right\} - \frac{3\mu q_0}{5(1-\mu)}, \\ \sigma_y &= \frac{6k}{h^2}\left\{\left(x^2-ax\right)^2\left(6y^2-6by+b^2+\frac{12}{5}h^2\right) + \left(6x^2-6ax+a^2\right)\right. \\ &\quad \cdot \left.\left[\mu\left(y^2-by\right)^2 + \frac{2h^2\left(6y^2-6by+b^2\right)}{5}\right]\right\} - \frac{3\mu q_0}{5(1-\mu)}. \end{aligned} \tag{12}$$

*3.2.2. First Breaking Interval of the Main Roof and Its Mechanical Characteristics.* According to the stress function calculated in Section 3.2.1, at $(x, y) = (0, b/2)$ and $(x, y) = (a, b/2)$, both $\sigma_x$ and $\sigma_y$ reach their peak negative values (that is, $\sigma_{x\ \max}$ and $\sigma_{y\ \max}$ are tensile stresses, $\sigma_{x\ \max} > \sigma_{y\ \max}$). Both are located at the centers of the long sides in the TPMM. $\sigma_{x\ \max}$ and $\sigma_{y\ \max}$ are given, respectively, as follows:

$$\begin{aligned} \sigma_{x\ \max} &= \frac{6k}{h^2}\left[\frac{b^4}{16}\left(a^2+\frac{12}{5}h^2\right) - \frac{1}{5}a^2b^2h^2\right] - \frac{3\mu q_0}{5(1-\mu)}, \\ \sigma_{y\ \max} &= \frac{6k}{h^2}\left(\frac{1}{16}\mu a^2b^4 - \frac{1}{5}a^2b^2h^2\right) - \frac{3\mu q_0}{5(1-\mu)}. \end{aligned} \tag{13}$$

If $\sigma_{x\ \max}$ in the main roof reaches the tensile strength $R_T$ (i.e.,$\sigma_{x\ \max} = R_T$), the long side with fixed support in the TPMM undergoes the first tensile failure. According to the geological conditions for the FMC, the basic parameters $R_T = 4.24$ MPa, $h = 13.3$ m, $q_0 = 0.554$ MPa, $\mu = 0.22$, and $b =$

320 m are substituted into the above formulas to estimate the first breaking interval of the main roof as $a = 40.6$ m.

Below, we analyze the mechanical characteristics of the main roof upon first weighting in the FMC by plotting the deflection and stress distribution of the main roof upon the first breaking using the Matlab software program based on the parameters calculated above. The results are shown in Figures 3–5.

As shown in Figure 3, the deflection of the main roof under fixed support on the four sides had a symmetric distribution about the goaf center. The largest deflection occurred in the center, and the deflection decreased gradually towards the periphery. The largest defection at the center of the goaf $(a/2, b/2)$ reached 1.25 mm.

As shown in Figure 4, the stress $\sigma_x$ in the main roof under the condition of fixed support on the four sides had an axisymmetric distribution about the goaf center with coordinates $(a/2, b/2)$, where the stress $\sigma_x$ in the main roof reached its maximum ($\sigma_{x\ \max} = 0.7$ MPa), indicating the largest compressive stress at this position. At the centers of the two long sides in the goaf, that is, at $(0, b/2)$ and $(a, b/2)$, the stress $\sigma_x$ in the main roof reached the peak negative value ($\sigma_{x\ \max} = 4.24$ MPa), indicating the largest tensile stress in this position. Besides, the tensile stress $\sigma_x$ already reached the ultimate tensile strength of the main roof. Therefore, tensile failure of the main roof occurred at the centers of the goaf's long sides.

As shown in Figure 5, stresses $\sigma_y$ and $\sigma_x$ in the main roof under the boundary condition of fixed support on four sides also had an axisymmetric distribution about the goaf center. At the center of the goaf $(a/2, b/2)$, the stress $\sigma_y$ in the main roof reached the largest positive value ($\sigma_{y\ \max} = 0.28$ MPa), indicating the largest compressive stress at this position. At the centers of the two long sides in the goaf, i.e., $(0, b/2)$ and $(a, b/2)$, the stress $\sigma_y$ in the main roof reached the largest negative value ($\sigma_{y\ \max} = 0.82$ MPa), indicating the largest tensile stress in this position. However, the tensile stress $\sigma_y$ did not reach the ultimate tensile strength of the main roof. Given the above, the failure of the main roof was not caused by the stress $\sigma_y$.

### 3.3. Mechanical Analysis of the Periodic Breaking Characteristics of the Main Roof

*3.3.1. Theoretical Analysis of the Mechanical Model for the Periodic Breaking of the Main Roof.* The governing equation for the boundary condition of fixed support on three sides and simple support on one side before the periodic breaking of the main roof in the FMC can be written as follows:

$$\begin{cases} \omega\big|_{x=0,x=a} = 0, \\ \dfrac{\partial^2\omega}{\partial x^2}\Big|_{x=0} = 0, \\ \dfrac{\partial\omega}{\partial x}\Big|_{x=a} = 0, \\ \omega\big|_{y=0,y=b} = 0, \\ \dfrac{\partial\omega}{\partial y}\Big|_{y=0,y=b} = 0. \end{cases} \tag{14}$$

Under the boundary condition of fixed support on three sides and simple support on one side, we derive the following deflection equation that satisfies the boundary conditions:

$$\omega = cx\left(x^2 - a^2\right)^2\left(y^2 - by\right)^2. \tag{15}$$

Substituting Equation (15) and $q_0$ into Equation (1), we can calculate the coefficient $c$ by the Matlab software program:

$$c = \frac{8085q_0}{128Da\left(336a^4 + 176a^2b^2 + 165b^4\right)}. \tag{16}$$

Substituting Equation (16) into Equation (15), we can derive the deflection function under the condition of fixed support on the three sides and simple support on one side for the main roof:

$$\omega = \frac{8085q_0x\left(x^2 - a^2\right)^2\left(y^2 - by\right)^2}{128Da\left(336a^4 + 176a^2b^2 + 165b^4\right)}. \tag{17}$$

Substituting Equation (17) into Equations (3)–(6), we can derive the shear stress function and the bending moment function of the main roof as follows:

$$\begin{aligned} Q_x &= k\left[\left(30x^2 - 6a^2\right)\left(y^2 - by\right)^2 + \left(x^2 - a^2\right)\left(5x^2 - a^2\right)\left(6y^2 - 6by + b^2\right)\right], \\ Q_y &= 2k\left[x\left(x^2 - a^2\right)^2(6y - 3b) + \left(10x^3 - 6a^2x\right)\left(y^2 - by\right)(2y - b)\right], \\ M_x &= k\left\{\left(y^2 - by\right)^2\left(10x^3 - 6a^2x + 12h^2x\right) + \left(6y^2 - 6by + b^2\right)\right. \\ &\quad \left.\cdot\left[\mu x\left(x^2 - a^2\right)^2 + \frac{4h^2\left(5x^3 - 3a^2x\right)}{5}\right]\right\} - \frac{\mu q_0h^2}{10(1-\mu)}, \\ M_y &= k\left\{x\left(x^2 - a^2\right)^2\left(6y^2 - 6by + b^2 + \frac{12}{5}h^2\right) + \left(5x^3 - 3a^2x\right)\right. \\ &\quad \left.\cdot\left[2\mu\left(y^2 - by\right)^2 + \frac{4h^2\left(6y^2 - 6by + b^2\right)}{5}\right]\right\} - \frac{\mu q_0h^2}{10(1-\mu)}, \end{aligned} \tag{18}$$

where $k = -8085q_0/64a\left(336a^4 + 176a^2b^2 + 165b^4\right)$.

Substituting the abovementioned bending moment function into $\sigma = 6M/h^2$, we can obtain the corresponding stress function:

$$\begin{aligned} \sigma_x &= \frac{6k}{h^2}\left\{\left(y^2 - by\right)^2\left(10x^3 - 6a^2x + 12h^2x\right) + \left(6y^2 - 6by + b^2\right)\right. \\ &\quad \left.\cdot\left[\mu x\left(x^2 - a^2\right)^2 + \frac{4h^2\left(5x^3 - 3a^2x\right)}{5}\right]\right\} - \frac{3\mu q_0}{5(1-\mu)}, \\ \sigma_y &= \frac{6k}{h^2}\left\{x\left(x^2 - a^2\right)^2\left(6y^2 - 6by + b^2 + \frac{12}{5}h^2\right) + \left(5x^3 - 3a^2x\right)\right. \\ &\quad \left.\cdot\left[2\mu\left(y^2 - by\right)^2 + \frac{4h^2\left(6y^2 - 6by + b^2\right)}{5}\right]\right\} - \frac{3\mu q_0}{5(1-\mu)}. \end{aligned} \tag{19}$$

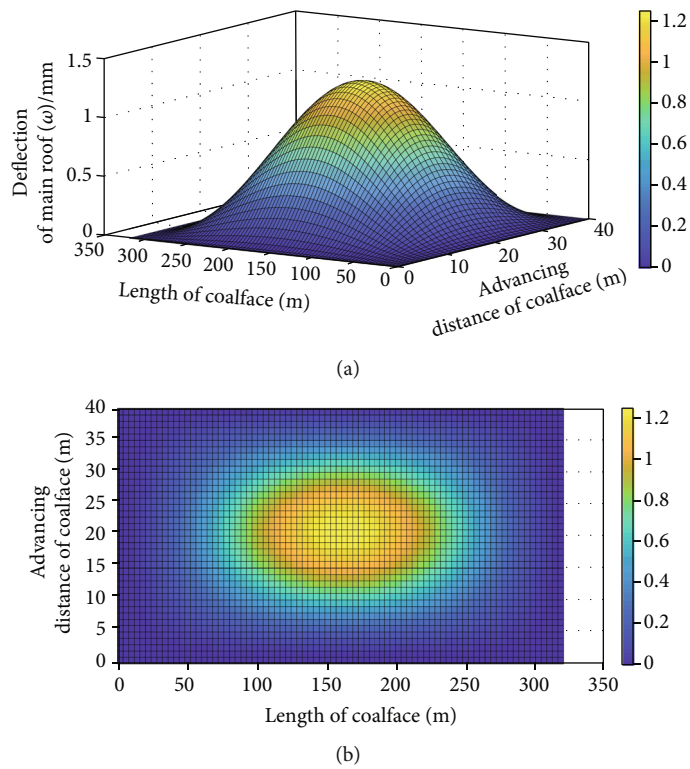


Figure 3: Deflection distribution of the main roof upon the first breaking: (a) three-dimensional distribution and (b) planar distribution.

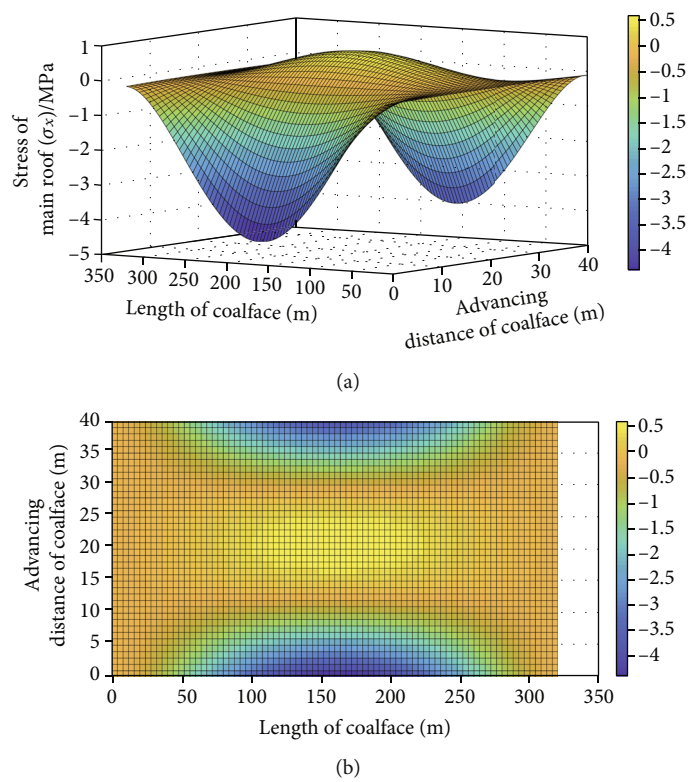


Figure 4: Distribution characteristics of the stress $\sigma_x$ upon the first breaking of the main roof: (a) three-dimensional distribution of the stress $\sigma_x$ and (b) planar distribution of the stress $\sigma_x$.

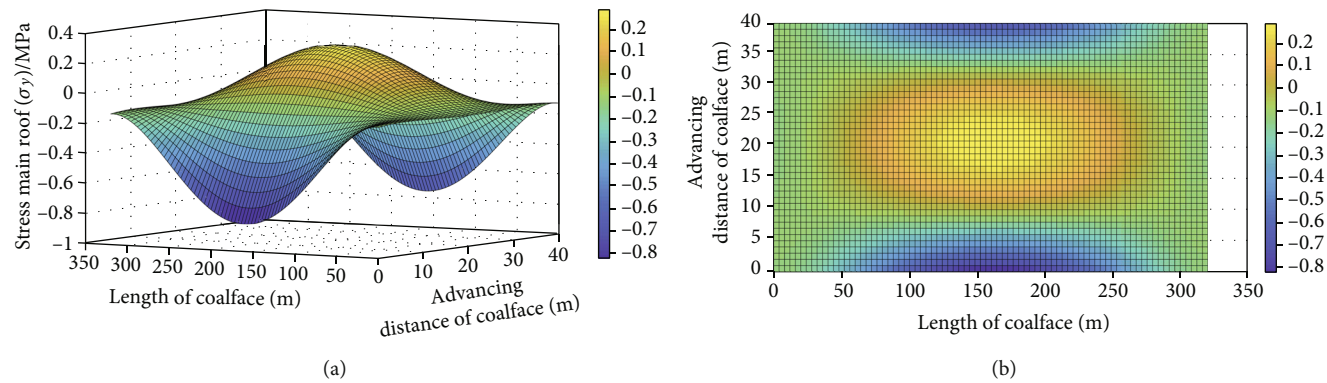


Figure 5: Distribution characteristics of stress $\sigma_y$ upon the first breaking of the main roof: (a) three-dimensional distribution of the stress $\sigma_y$ and (b) planar distribution of the stress $\sigma_y$.

*3.3.2. Periodic Breaking Interval of the Main Roof and Its Mechanical Characteristics.* According to the stress function calculated in Section 3.3.1, at $(x, y) = (a, b/2)$, both $\sigma_x$ and $\sigma_y$ both reach the largest negative value (that is, $\sigma_{x\ \max}$ and $\sigma_{y\ \max}$ are tensile stresses, $\sigma_{x\ \max} > \sigma_{y\ \max}$), indicating that both are located at the centers of the long sides with fixed support in the TPMM. Values of $\sigma_{x\ \max}$ and $\sigma_{y\ \max}$ are derived as follows:

$$\sigma_{x\ \max} = \frac{6k}{h^2}\left[\frac{ab^4\left(a^2+3h^2\right)}{4} - \frac{4h^2a^2b^2}{5}\right] - \frac{3\mu q_0}{5(1-\mu)},$$
$$\sigma_{y\ \max} = \frac{6k}{h^2}a^3b^2\left(\frac{\mu b^2}{4} - \frac{4h^2}{5}\right) - \frac{3\mu q_0}{5(1-\mu)}. \tag{20}$$

Thus, when $\sigma_{x\ \max}$ in the main roof reached the tensile strength $R_T$ (i.e.,$\sigma_{x\ \max} = R_T$), tensile failure occurred periodically at the long sides with fixed support in the TPMM. By substituting the basic parameters of the FMC into the above equations, we estimated the periodic breaking interval of the main roof as $a = 25.0$ m.

Similarly, we plotted the deflection and stress distributions of the main roof upon periodic breaking using the Matlab software program (Figures 6–8). Then, the mechanical characteristics of the main roof upon periodic weighting in the FMC were analyzed.

As shown in Figure 6, the deflection of the main roof had an axisymmetric distribution about the goaf center ($y = b/2$) under the boundary condition of fixed support on the three sides and simple support on one side. We observed the largest deflection at the center, with a gradual decrease towards the periphery. In the position ($\sqrt{5}a/5$, $b/2$) in the goaf, the main roof deflection reached a maximum of 0.36 mm.

As shown in Figure 7, the stress $\sigma_x$ in the main roof had an axisymmetric distribution about the goaf center ($y = b/2$) under the boundary condition of fixed support on the three sides and simple support on one side. At the center of the long side with fixed support in the goaf $(a, b/2)$, the stress $\sigma_x$ in the basic stress reached the peak negative value ($\sigma_{x\ \max} = 4.24$ MPa), indicating the largest tensile stress in this position. At this moment, the tensile stress $\sigma_x$ already reached the ultimate tensile strength of the main roof. Therefore, tensile failure of the main roof occurred at the centers of the long sides with fixed support in the goaf.

As shown in Figure 8, both stresses $\sigma_y$ and $\sigma_x$ in the main roof had an axisymmetric distribution about the goaf center ($y = b/2$) under conditions of fixed support on the three sides and simple support on one side. At ($\sqrt{5}a/5$, $b/2$) in the goaf, stress $\sigma_y$ reached the largest positive value ($\sigma_{y\ \max} = 0.12$ MPa), indicating the largest compressive stress in this position. At the center of the goaf long side $(a, b/2)$, the stress $\sigma_y$ in the main roof reached the largest negative value ($\sigma_{y\ \max} = 0.58$ MPa), indicating the largest tensile stress in this position. However, the tensile stress $\sigma_y$ did not reach the ultimate tensile strength in the main roof at this moment. It could be inferred that the stress $\sigma_y$ caused no failure in the main roof.

## 4. Field Measurement of Ground Pressure Behavior in the FMC

In this section, the working resistance of hydraulic supports in the FMC was studied during the stoping period. The working resistance variations of the hydraulic supports were characterized. We analyzed the first and periodic weighting patterns in the coalface and verified the feasibility of the proposed TPMM for the main roof breaking. On this basis, we evaluated the applicability of the hydraulic supports used in the coalface, offering valuable clues for roof management in the coalface.

*4.1. Field Measurement Plan for Ground Pressure.* A total of 25 measurement stations were installed along the dip direction of the coalface to analyze ground pressure behavior at different positions in the roof (Figure 9). The measurement stations were located at the following hydraulic supports: #4, #8, #15, #23, #30, #38, #46, #53, #60, #68, #76, #83, #92, #98, #106, #113, #120, #128, #136, #143, #150, #158, #166, #174, and #183. The YHY60W(A) support pressure gauges for mines developed by the Xuzhou Shengneng

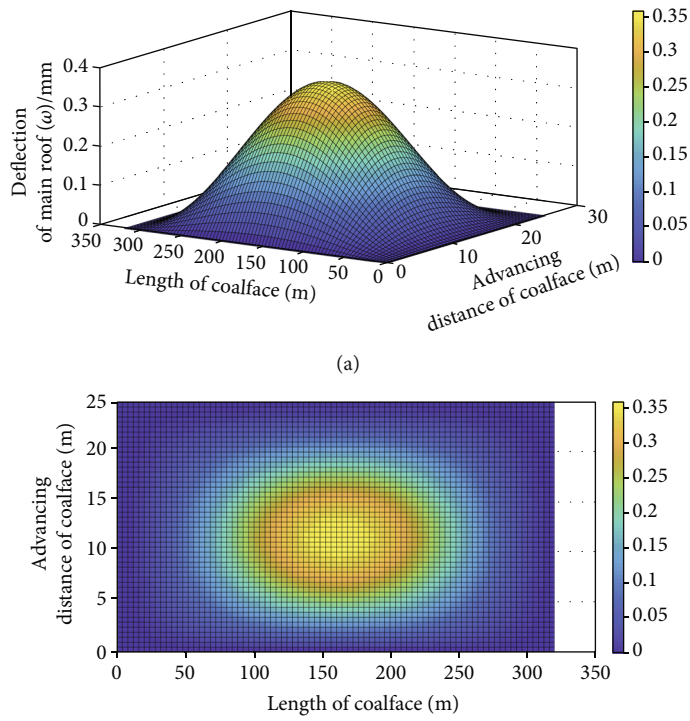


Figure 6: Characteristics of deflection distribution of the main roof upon periodic breaking: (a) three-dimensional distribution and (b) planar distribution.

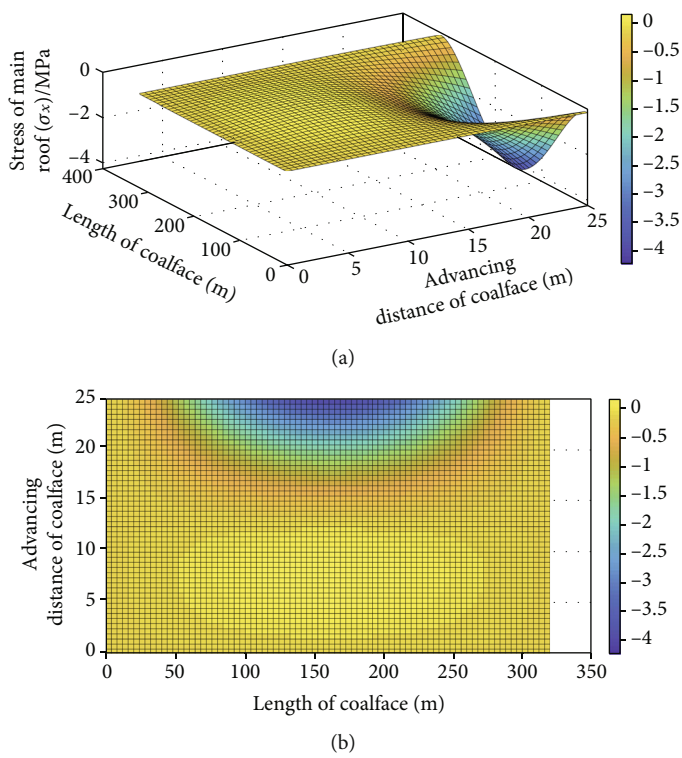


Figure 7: Distribution characteristics of stress $\sigma_x$ in the main roof upon periodic breaking: (a) three-dimensional distribution of the stress $\sigma_x$ and (b) planar distribution of stress $\sigma_x$.

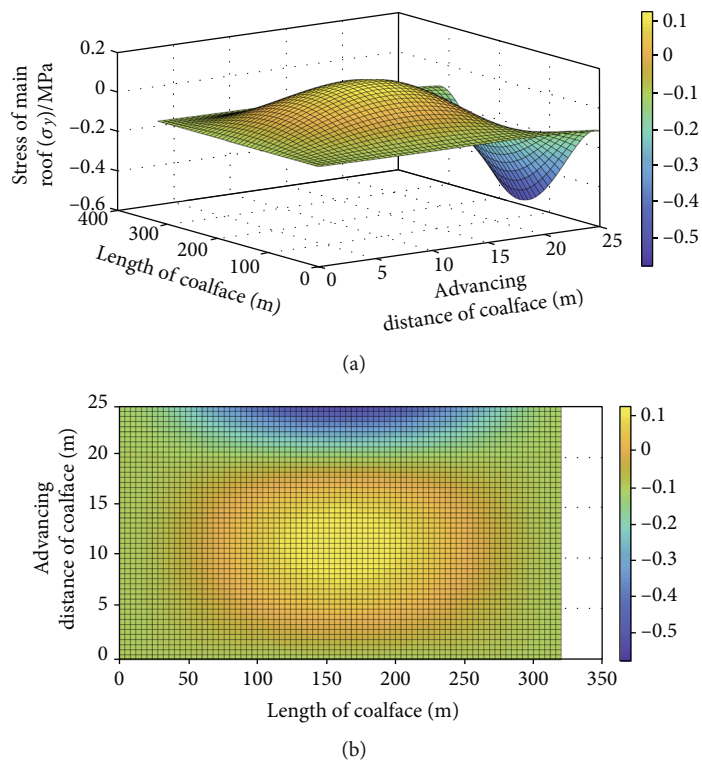


Figure 8: Distribution characteristics of stress $\sigma_y$ in the main roof upon periodic breaking: (a) three-dimensional distribution of the stress $\sigma_y$ and (b) planar distribution of the stress $\sigma_y$.

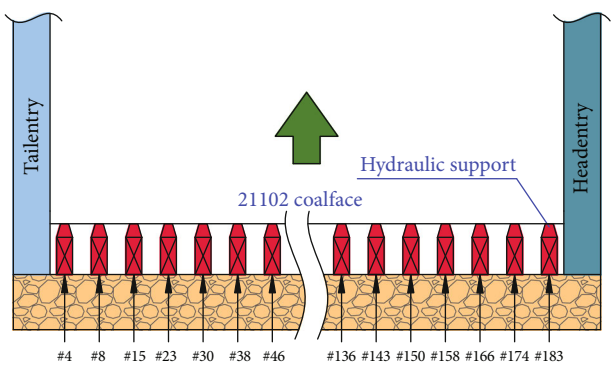


Figure 9: The layout of the measurement stations in the coalface.

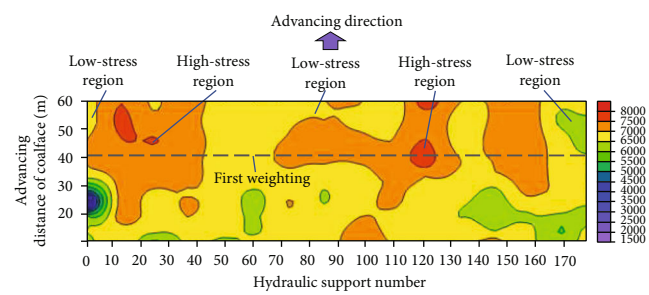


Figure 10: Distribution characteristics of the daily average working resistance of hydraulic supports during primary mining.

Technology Co., Ltd. were installed in the corresponding measurement stations for continuous monitoring of the working resistance of hydraulic supports.

*4.2. Analysis of the First Weighting Characteristics in the Coalface.* Generally speaking, weighting in the coalface can be more accurately performed using the circulation terminal resistance (CTR) of hydraulic supports. However, after installing and debugging the special ground pressure-monitoring system, the FMC had already advanced by 140 m. Therefore, the CTR could not be timely and accurately captured by the electrohydraulic control system embedded in the hydraulic supports. For this reason, we analyzed the first weighting of the main roof in the coalface according to the actual roof caving, time-weighted resistance (TWR) of the hydraulic supports, and daily maximum resistance (DMR) of the hydraulic supports.

During the primary mining of the FMC, when the coalface advanced from the open-off cut for about 12 m, the immediate roof in the middle of the coalface collapsed. As the coalface further advanced to 20 m, the entire immediate roof had collapsed, filling the goaf. When the coalface advanced to about 40 m, clear breaking sounds could be heard from the main roof. Thus, the occurrence of the first weighting of the coalface was confirmed. During the primary mining of the coalface, the overall distribution of the daily average working resistance of the hydraulic supports is monitored and plotted in Figure 10. From the coalface's head to its tail, the low-stress region, high-stress region, low-stress region, high-stress region, and low-stress region appeared successively. This was a saddle-shaped distribution, which was typical of the ultralong coalface.

Table 1: Judgment criteria for the first weighting in some hydraulic supports.

| No. | $\bar{P}_t$ | $\sigma_t$ | $P_t$ | $\bar{P}_{max}$ | $\sigma_{max}$ | $P_{max}$ |
|---|---|---|---|---|---|---|
| #8 | 6765 | 348 | 7113 | 7922 | 379 | 8301 |
| #46 | 6680 | 290 | 6970 | 7694 | 271 | 7965 |
| #92 | 6805 | 310 | 7115 | 7783 | 289 | 8072 |
| #120 | 7150 | 500 | 7650 | 8019 | 395 | 8414 |
| #174 | 6850 | 230 | 7080 | 7894 | 231 | 8125 |

$\bar{P}_t$: value of TWR; $\sigma_t$: standard deviation of TWR; $P_t$: JCTWR; $\bar{P}_{max}$: mean value of DMR; $\sigma_{max}$: standard deviation of DMR; $P_{max}$: JCDMR.

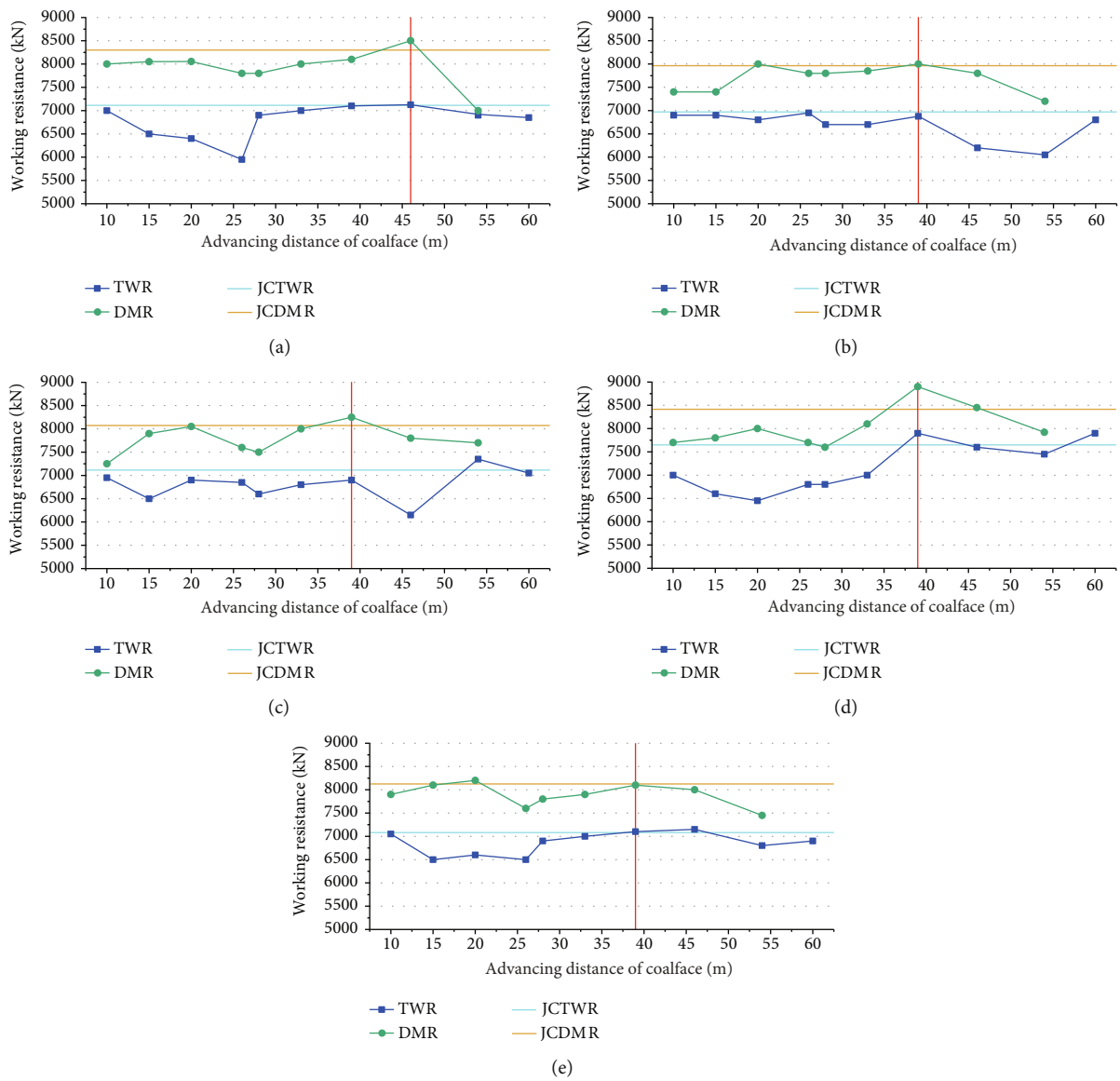


Figure 11: Variation curves of working resistance in some hydraulic supports upon first weighting: (a) #8 hydraulic support, (b) #46 hydraulic support, (c) #92 hydraulic support, (d) #120 hydraulic support and (e) #174 hydraulic support.

The judgment criteria of time-weighted resistance (JCTWR) and the judgment criteria of daily maximum resistance (JCDMR) of some hydraulic supports in the coalface were calculated for the first weighting, as shown in Table 1. The variation curves of the working resistance of hydraulic supports are presented in Figure 11 (the red vertical line indicates the position of the first weighting in the coalface).

According to Table 1 and Figure 11, the first weighting interval of the main roof in the FMC was 38.5-45.9 m, with an average of 41.4 m, which agreed with the field

Table 2: Judgment criteria for periodic weighting in some hydraulic supports.

| No. | $\bar{P}_t$ | $\sigma_t$ | $P_t$ | $\bar{P}_m$ | $\sigma_m$ | $P_m$ |
|---|---|---|---|---|---|---|
| #4 | 7635 | 680 | 8315 | 8794 | 663 | 9457 |
| #15 | 8537 | 534 | 9071 | 9502 | 508 | 10010 |
| #30 | 8999 | 520 | 9519 | 9810 | 573 | 10383 |
| #46 | 8905 | 434 | 9339 | 9731 | 473 | 10204 |
| #60 | 8957 | 475 | 9432 | 9873 | 633 | 10506 |
| #83 | 8840 | 379 | 9219 | 9729 | 448 | 10177 |
| #92 | 8552 | 708 | 9260 | 9547 | 486 | 10033 |
| #98 | 8893 | 363 | 9256 | 9695 | 365 | 10060 |
| #113 | 8844 | 436 | 9280 | 9676 | 505 | 10181 |
| #128 | 8595 | 591 | 9186 | 9516 | 442 | 9958 |
| #136 | 9259 | 667 | 9926 | 10245 | 783 | 11028 |
| #150 | 8664 | 561 | 9225 | 9614 | 590 | 10204 |
| #166 | 7590 | 543 | 8133 | 8652 | 687 | 9339 |
| #174 | 7419 | 830 | 8249 | 8169 | 690 | 8859 |

$\bar{P}_m$: mean value of CTR; $\sigma_m$: standard deviation of CTR; $P_m$: JCCTR.

observation. The main roof of the FMC was composed of hard and thick sandstone. Deep-hole presplit blasting has been performed for the open-off cut roof to prevent roof disaster caused by the extensive roof overhang. Therefore, the first weighting of the coalface had low intensity, and the safety valves of the hydraulic supports did not open extensively. The dynamic load factor of the hydraulic supports during the first weighting of the coalface was 1.04-1.18, with an average of 1.08, which values were relatively small.

*4.3. Analysis of the Periodic Weighting Characteristics in the Coalface.* Field measurement data were collected from the special ground pressure monitoring system installed in the hydraulic supports. Periodic weighting was analyzed as the coalface advanced from 140 to 400 m. The judgment criteria of time-weighted resistance (JCTR) and the judgment criteria of circulation terminal resistance (JCCTR) of some hydraulic supports were calculated; the results are shown in Table 2. The variation curves of the working resistance of some hydraulic supports are shown in Figure 12 (the red vertical line indicates the position of the periodic weighting in the coalface).

As shown in Table 2 and Figure 12, as the FMC advanced from 140 to 400 m (i.e., by a distance of 260 m), 10-13 events of periodic weighting occurred in total. The minimum, average, and maximum weighting intervals were 11.6, 22.0, and 38.7 m. The dynamic load factor of the hydraulic supports during the periodic weighting of the coalface was 1.03-1.09, with an average of 1.06. This dynamic load factor was relatively small.

*4.4. Applicability Evaluation of the Hydraulic Supports Used.* The operational resistance data of the hydraulic supports were analyzed as the FMC advanced from 0 to 400 m. The distribution of the daily average working resistance of the hydraulic supports is shown in Figure 13. From the head to the tail of the coalface, hydraulic supports' daily average working resistance presented a "saddle-shaped" distribution similar to the primary mining of the coalface (low-stress region, high-stress region, low-stress region, high-stress region, and low-stress region). Along the advanced direction of the coalface, there were three types of regions, classified by their daily average working resistance, namely, low-stress region, transition region, and high-stress region.

(1) *Low-Stress Region (0-100 m).* The overburden failure in the coalface was extremely insufficient within this region. The daily average working resistance of hydraulic supports was generally below 7000 kN and changed little. No significant coal wall spalling was observed during the coalface advance.

(2) *Transition Region (100-300 m).* Within this region, the degree of overburden failure in the coalface grew with the coalface advance. The daily average working resistance of hydraulic supports gradually increased.

(3) *High-Stress Region (Beyond 300 m).* The overburden failure in the coalface already became sufficient within this region. The daily average working resistance of hydraulic supports was generally above 8000 kN. Significant coal wall spalling was observed during the coalface advance.

The frequency distribution of working resistance usually characterizes the operational performance of hydraulic supports. A reasonable working resistance distribution of hydraulic supports is a near-normal distribution [30]. A higher share of low working resistance usually indicates a lower efficiency of the hydraulic supports. Besides, the rated working resistance margin is large under the above situation. By contrast, a higher share of the high working resistance indicates that the hydraulic supports mostly work at a high load. The rated working resistance is lower and cannot meet the actual support demand on-site. The frequency distribution of the working resistance of hydraulic supports was analyzed statistically as the FMC advanced from 0 to 400 m. It

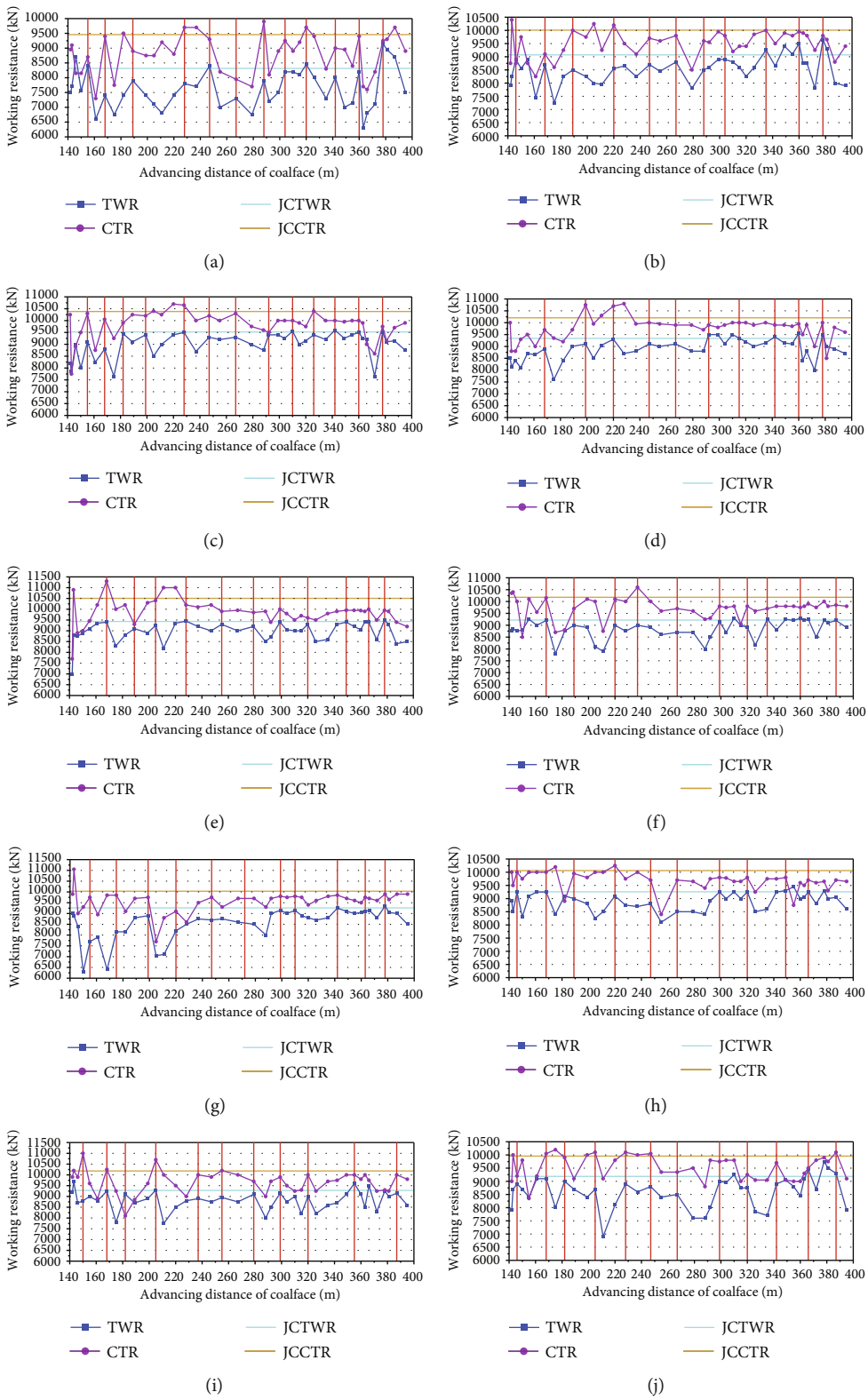


Figure 12: Continued.

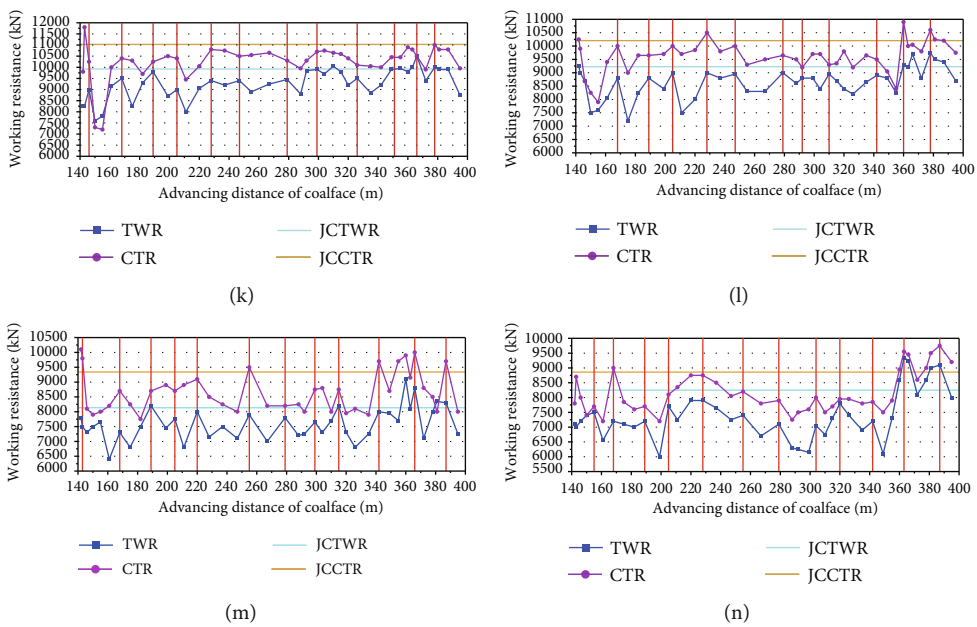


Figure 12: Variation curves of working resistance of some hydraulic supports upon periodic weighting: (a) #4 hydraulic support, (b) #15 hydraulic support, (c) #30 hydraulic support, (d) #46 hydraulic support, (e) #60 hydraulic support, (f) #83 hydraulic support, (g) #92 hydraulic support, (h) #98 hydraulic support, (i) #113 hydraulic support, (j) #128 hydraulic support, (k) #136 hydraulic support, (l) #150 hydraulic support, (m) #166 hydraulic support, and (n) #174 hydraulic support.

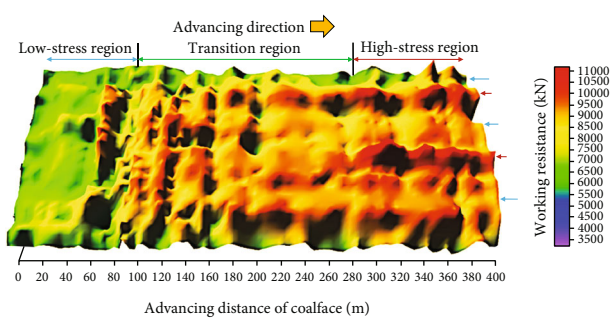


Figure 13: Distribution characteristics of the daily average working resistance of hydraulic supports.

yielded 0.4% for the 0-2000 kN interval, 0.2% for the 2000-4000 kN interval, 1.1% for the 4000-6000 kN interval, 28.2% for the 6000-8000 kN interval, 65.3% for the 8000-10000 kN interval, and 4.8% for the interval above 10000 kN. According to these results, high working resistance (above 8000 kN) had the dominating share of 70.1%. This indicated that the hydraulic supports generally worked at high loads with a small margin of the rated working resistance.

## 5. Conclusions

(1) The proposed TPMM of the main roof breaking predicted that the first and periodic weighting intervals of the main roof caused by the internal stress $\sigma_x$ in the rock strata were 40.6 and 25.0 m, respectively. The tensile failure first started in the goaf from the center of the long side with fixed support

(2) Field measurements of ground pressure showed that the first weighting interval of the main roof in the FMC was 38.5-45.9 m, with an average of 41.4 m. The periodic weighting interval was 11.6-38.7 m, with an average of 22.0 m. The discrepancy between the model predictions and field data was quite small. The above results indicated that the TPMM was applicable to the particular geological conditions of the FMC

(3) The estimation of the daily average working resistance of hydraulic supports exhibited a saddle-shaped pattern along the coalface dip direction, with the following sequence order: low-stress region, high-stress region, low-stress region, high-stress region, and low-stress region, judging by the daily average working resistance. This saddle-shaped distribution was typical of the ultralong coalface. Along the advanced direction of the coalface, the daily average working resistance could be classified into three types of regions by the low-stress region, transition region, and high-stress region

(4) Analysis of the working resistance frequency distribution revealed that the ZY10000-16/32D two-column shield-type hydraulic supports could adapt to the geological conditions under which the FMC was mined. However, the hydraulic supports generally experienced high loads, with an insufficient margin of the rated working resistance (i.e., 10000 kN). Therefore, enhanced roof management in the presence of special geological structures (e.g., faults and goaf passages) during the coalface mining is strongly recommended

## Data Availability

The data used to support the findings of this study are included within the article.

## Conflicts of Interest

The authors declare that there are no conflicts of interest regarding the publication of this paper.

## Acknowledgments

This work was financially supported by the National Natural Science Foundation of China (No. 51874278), the "Six Talent Peaks" Project of Jiangsu Province (No. JNHB-087), the Postgraduate Research and Practice Innovation Program of Jiangsu Province (Nos. KYCX21_2339 and KYCX21_2247), and the Independent Research Project of State Key Laboratory of Coal Resources and Safe Mining (No. SKLCRSM2020X04). We wish to thank the HCM in HMA, China, for supporting field help to conduct this important study.

## References

[1] D. S. Zhang, W. P. Li, X. P. Lai, G. W. Fan, and W. Q. Liu, "Development on basic theory of water protection during coal mining in northwest of China," *Journal of China Coal Society*, vol. 42, no. 1, pp. 36–43, 2017.

[2] D. L. Jiang and H. Cheng, "Medium and long term forecast and prospect of coal consumption in China," *Coal Economic Research*, vol. 40, no. 7, pp. 16–21, 2020.

[3] M. D. Woodworth, "Disposable Ordos: The making of an energy resource frontier in western China," *Geoforum*, vol. 78, no. 1, pp. 133–140, 2017.

[4] W. Z. Liu, Z. P. Guo, S. W. Niu, J. F. Hou, F. Y. Zhang, and C. Q. He, "Mechanical properties and damage evolution behavior of coal-fired slag concrete under uniaxial compression based on acoustic emission monitoring technology," *Journal of Materials Research and Technology*, vol. 9, no. 5, pp. 9537–9549, 2020.

[5] Q. Ma, Y. L. Tan, X. S. Liu, Q. H. Gu, and X. B. Li, "Effect of coal thicknesses on energy evolution characteristics of roof rock-coal-floor rock sandwich composite structure and its damage constitutive model," *Composites Part B: Engineering*, vol. 198, 2020.

[6] H. G. Nie, F. C. Dong, W. K. Zhao, and Z. Xi, "Coal-Tbearing strata sequence stratigraphic fatures and coal accumulation pattern analysis in Dongsheng coalfield -a case study of Abuhai exploration area in Dongsheng coalfield," *Coal Geology of China*, vol. 23, no. 2, pp. 10–16, 2011.

[7] X. M. Wang, X. M. Wang, S. D. Pan et al., "Occurrence of analcime in the middle Jurassic coal from the Dongsheng Coalfield, northeastern Ordos Basin, China," *International Journal of Coal Geology*, vol. 196, no. 1, pp. 126–138, 2018.

[8] Y. Q. Jiao, S. M. Wang, L. M. Fan, L. Q. Wu, H. Rong, and F. Zhang, "Key elements and framework model of groundwater system in Jurassic coal measures of Ordos Basin," *Journal of China Coal Society*, vol. 45, no. 7, pp. 2411–2422, 2020.

[9] Q. X. Huang, *Strata Control of Shallow Coal Seam Longwall Mining*, Science Press, Beijing, 2019.

[10] S. S. Peng, H. M. Li, Y. Zhou et al., *Study on Strata Control in Shendong and Junggar Mining Areas*, Science Press, Beijing, 2015.

[11] D. S. Zhang, G. W. Fan, X. F. Wang, W. Zhang, and H. L. Liu, *Study on Overburden Activity Law and Its Control Technology of Shallow Coal Seam Mining in Gully-Growth-Wide Mining Area*, China University of Mining and Technology Press, Xuzhou, 2014.

[12] S. G. Cao, H. J. Jiang, and Y. Zhang, *Study on the Breaking and Control of Key Strata under Short-Wall Mining in Shallow Seam*, China University of Mining and Technology Press, Xuzhou, 2019.

[13] Y. H. Zhao and X. M. Song, "Stability analysis and numerical simulation of hinged arch structure for fractured beam in super-long mining workface under shallow seam," *Rock and Soil Mechanics*, vol. 37, no. 1, pp. 203–209, 2016.

[14] J. G. Ning, X. S. Liu, Y. L. Tan, M. Zhang, and L. S. Zhang, "Fracture structure model of weakly cemented roof in shallow seam," *Journal of Mining & Safety Engineering*, vol. 31, no. 4, pp. 569–574, 2014.

[15] G. X. Xie, H. Fan, and L. Wang, "Evolution law and engineering application of surrounding rock force chain in shallow coal seam working face," *Journal of China Coal Society*, vol. 44, no. 10, pp. 2945–2952, 2019.

[16] X. W. Yin, "Cutting block structure model of overburden with shallow buried coal seam and ultra-large mining height working face," *Journal of China Coal Society*, vol. 44, no. 7, pp. 1961–1970, 2019.

[17] B.-F. Wa, L. Bing, K.-M. Su et al., "Research on overlying strata response and control during typical shallow coal seam longwall mining," *Rock and Soil Mechanics*, vol. 38, no. 9, pp. 2693–2700, 2017.

[18] J. C. Wang and Z. H. Wang, "Stability of main roof structure during the first weighting in shallow high-intensity mining face with thin bedrock," *Journal of Mining & Safety Engineering*, vol. 32, no. 2, pp. 175–181, 2015.

[19] C. S. Di, X. Ding, and H. Huang, "Practice of exploration and discharge technology of roof water in deep Jurassic coal seam: with Hulusu coal mine in Hujiert mine area as example," *Coal Geology & Exploration*, vol. 44, no. 6, pp. 96–100, 2016.

[20] S. J. Su, "Research on technology of preventing mine rock burst of roadways near gob when fully-mechanized over anticlinal structure," *Coal Science and Technology*, vol. 48, no. 3, pp. 120–125, 2020.

[21] J. Sun, "Study on deep coal roof Qilizhen sandstone aquifer water yield property in Hujiert mining area," *Coal Geology of China*, vol. 33, no. 4, pp. 62–67, 2021.

[22] Q. Wu, Y. Z. Liu, W. F. Zhou et al., "Evaluation of water inrush vulnerability from aquifers overlying coal seams in the Menkeqing coal mine, China," *Mine Water and the Environment*, vol. 34, no. 3, pp. 258–269, 2015.

[23] J. Wang, J. Ning, L. Jiang, J. Q. Jiang, and T. Bu, "Structural characteristics of strata overlying of a fully mechanized longwall face: a case study," *Journal of the Southern African Institute of Mining and Metallurgy*, vol. 118, no. 11, 2018.

[24] G. L. Ding, X. H. Lu, S. G. Wu, and Y. Q. Liu, "Sturdy on ground pressure law and support adaptability of deep-buried and ultra-long fully-mechanized longwall mining face," *Coal Science and Technology*, vol. 49, no. 3, pp. 43–48, 2021.

[25] W. Zhang, X. Qu, C. Li et al., "Fracture analysis of multi-hard roofs based on microseismic monitoring and control

techniques for induced rock burst: a case study," *Arabian Journal of Geosciences*, vol. 12, no. 24, 2019.

[26] S. L. Yang, J. C. Wang, and L. H. Li, "Deformation and fracture characteristics of key strata based on the medium thick plate theory," *Journal of China Coal Society*, vol. 45, no. 8, pp. 2718–2727, 2020.

[27] B. L. Fu and W. F. Tan, "The reciprocal theorem method for solving bending problems of thick rectangular plates," *Applied Mathematics and Mechanics*, vol. 16, no. 4, pp. 367–379, 1995.

[28] E. Reissner, "The effect of transverse shear deformation on the bending of elastic plates," *Journal of Applied Mechanics*, vol. 12, no. 2, pp. A69–A77, 1945.

[29] V. L. Salerno and M. A. Goldberg, "Effect of shear deformations on the bending of rectangular plates," *Journal of Applied Mechanics*, vol. 27, no. 1, pp. 54–58, 1960.

[30] W. H. Zha, X. Z. Hua, J. C. Wang, H. F. Zheng, N. G. Wang, and X. Liu, "Study on strata movement rules and hydraulic support selection for fully-mechanized working face with large mining height of extra," *Journal of Safety Science and Technology*, vol. 10, no. 8, pp. 75–80, 2014.